2

Unimolecular Dissociations in Mass Spectrometry

Toshihide Nishimura

2.1 Statistical Theory of Unimolecular Dissociation

Gaseous reactions can be categorized as (a) thermal reactions in which activation and deactivation of a molecule proceed via molecule/molecule collisions, and (b) unimolecular reactions of highly excited molecules or ions taking place without collisions:

$$\begin{array}{rcll} \mathrm{A}+\mathrm{M} & \xrightarrow[{[k_1]}]{} & \mathrm{A}^*+\mathrm{M} & \text{(collisional activation)}\\ \mathrm{A}^*+\mathrm{M} & \xrightarrow[{[k_{-1}]}]{} & \mathrm{A}+\mathrm{M} & \text{(collisional deactivation)}\\ \mathrm{A}^* & \xrightarrow[{[k_2]}]{} & \text{Product} & \text{(unimolecular reaction).} \end{array} \qquad (2.1)$$

Thus, unimolecular reaction of a molecule A can be described by the Rice–Ramsperger–Kassel–Marcus (RRKM) theory [1–6], in which a molecule is considered as a set of harmonic oscillators which can interact with each other by exchanging energy freely. The unimolecular reaction rate $k(E)$ is derived by statistical assumptions as follows (Fig. 2.1):

1. An excited molecule A^* with internal energy E can assume all possible internal states, and A^* undergoes unimolecular reactions when it goes beyond the critical state, C. This critical state is often referred to as a transitional state.
2. The internal redistribution of the initial vibrational excitation modes to other possible vibration modes in an activated molecule A^* occurs much faster than unimolecular reaction.

In this model, it is assumed that the initial energy distribution of a reactant can be described statistically and that energy is not exchanged between molecular assemblies. Such assemblies are termed “microcanonical.” Since each state of A^* at a given energy has the same probability with respect to unimolecular reaction, the microcanonical ensemble is conserved via a unimolecular reaction. Therefore, the rate constant of a unimolecular reaction can be described merely using $k(E)$. To be comprehensive, simply replace the term unimolecular reaction with “unimolecular

---

T. Nishimura (✉)
Biosys Technologies Inc. & Tokyo Medical University, 2012-865 Sasagi, Tsukuba, Ibaraki 305-0043, Japan
e-mail: linne300@hotmail.co.jp

K. Hiraoka (ed.), *Fundamentals of Mass Spectrometry*, DOI 10.1007/978-1-4614-7233-9_2,

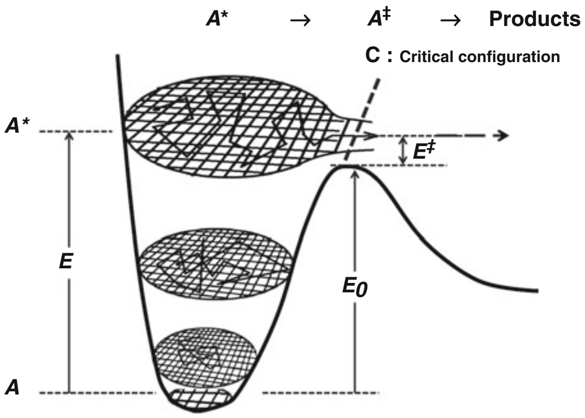

Fig. 2.1 A schematic potential surface of unimolecular reaction (dissociation) of a molecule A, where representative internal-state assemblies at several energies E is shown as a cross section comprising individual states (*squares*). A^* and $A^\ddagger$ are the molecules at excited state and critical configuration. E_0 and $E^\ddagger$ are, respectively, the activation and internal excess energies via unimolecular reaction

dissociation." From the assumption of rapid redistribution of internal vibrational energy, it follows that an excited molecule A^* at a given energy E has a random lifetime distribution [6] given by

$$P(\tau) = k(E)\ \exp(-k(E)\ \tau). \tag{2.2}$$

There is no preference regarding the dissociation of any specific molecule or of its possible radioactive decay.

For a molecular state with a classical energy E, the number of states, N, with one degree of freedom for the momentum p and position q is described as

$$N = \frac{\mathrm{d}p\,\mathrm{d}q}{h}, \tag{2.3}$$

where h is Planck's constant. That is, the phase space volume per unit state equals h, and then the total sum of state, $G(E)$, at a given energy E becomes the total phase space V divided by h:

$$G(E) = \frac{V}{h}. \tag{2.4}$$

When one harmonic oscillator with a vibrational frequency of ν is considered, its classical *Hamiltonian equation* is given as

$$H(p, q) = \frac{p^2}{2} + \frac{\lambda q^2}{2}, \tag{2.5}$$

where $\lambda = 4\pi^2\,\nu^2$. Then, the phase space volume is calculated by

$$V = \int_{H=0}^{H=E} \int \mathrm{d}p\mathrm{d}q = \pi ab \tag{2.6}$$

which is equal to the “ellipse” area with the semimajor and semiminor axes, a and b, given as $b = (2E)^{1/2}$ and $a = (2E/\lambda)^{1/2}$. It then becomes

$$V = \frac{E}{v}. \tag{2.7}$$

Therefore, from (2.4) the number of classical states is expressed as

$$G(E) = \frac{E}{h\nu}. \tag{2.8}$$

For the Hamiltonian expanded to the harmonic oscillators ($n = s$)

$$H(p, q) = \sum_{i=1}^{s} \left(\frac{p^2}{2} + \frac{\lambda_i {q_i}^2}{2} \right), \tag{2.9}$$

its corresponding volume of phase space is similarly obtained by

$$V_s = \frac{E^s}{s! \sum_{i=1}^{s} \nu_i}. \tag{2.10}$$

Then, the state sum becomes

$$G\,(E) = \frac{V_s}{h} = \frac{E^s}{s! \sum_{i=1}^{s} h\nu_i}, \tag{2.11}$$

and so the state density is given as follows:

$$N(E) = \frac{\mathrm{d}G(E)}{\mathrm{d}E} = \frac{E^{s-1}}{(s-1)! \sum_{i=1}^{s} h\nu_i}. \tag{2.12}$$

For a molecule comprising harmonic oscillators ($n = s$) having a total energy E, the probability that an internal excess energy, $E - E_0$, beyond a critical energy E_0 in the vibrational modes will lead to facile dissociation is given by

$$\frac{N(E - E_0)}{N(E)} = \left(\frac{E - E_0}{E} \right)^{s-1}. \tag{2.13}$$

Therefore, the classical rate constant $k(E)$ can be expressed using this probability multiplied by the frequency ν of a specific vibrational mode along reaction coordinate [7]:

$$k(E) = \nu \left(\frac{E - E_0}{E} \right)^{s-1}, \tag{2.14}$$

which is known as the classical rate constant (Kassel’s equation).

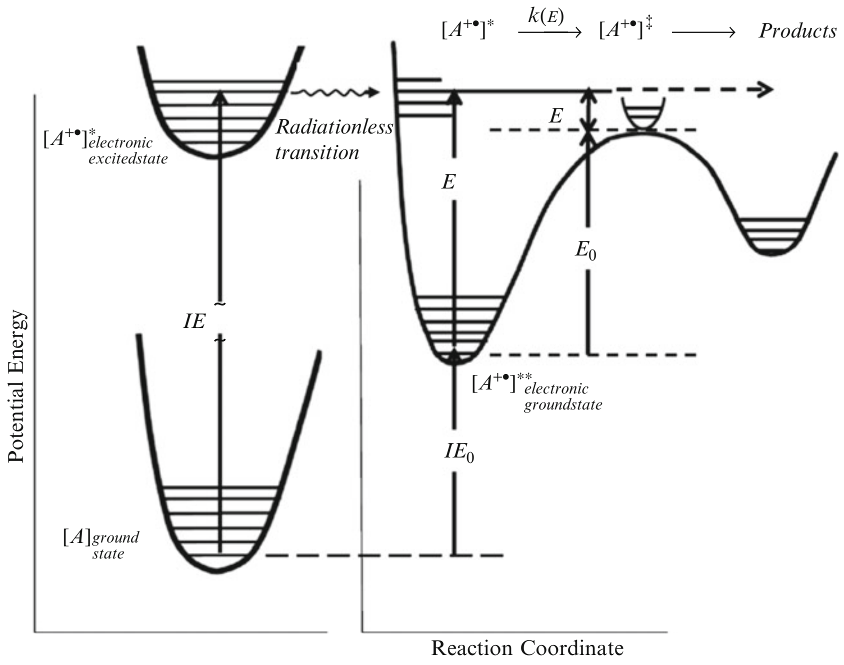

Fig. 2.2 A schematic diagram on unimolecular dissociation based on QET. Ionization of the molecule [A] and internal conversion (radiationless transition) of initially excited electronic states to the ionic ground state $[A^{+\bullet}]$ is followed by unimolecular dissociation

In a mass spectrometer, molecular ions are produced via ionization and are separated according to their *m*/*z* prior to detection. In simple cases such as electron ionization (EI) and photoionization (PI), an isolated neutral molecule in the ground state, $[\mathrm{A}]_{\mathrm{ground}}$, is first excited to its electronically excited ionic state, $[\mathrm{A}^{+\bullet}]^{*}_{\mathrm{electronic}}$, following the so-called *Franck–Condon principle*. The Franck–Condon principle states that ionization takes place at constant internuclear distance because the removal of an electron (•) occurs within 10^{-16} s and so is much faster than a vibrational oscillation, 10^{-13}–10^{-14} s. This electronically excited molecular ion then undergoes its unimolecular reaction (dissociation) to dissipate excitation energy. The modern theory of mass spectra, the *quasi-equilibrium theory* (QET), is introduced by Rosenstock et al. [8] based on the following main hypotheses:

1. An electronically excited molecular ion is rapidly converted via radiationless transition (internal conversion) to its electronic ground state ion $[\mathrm{A}^{+\bullet}]^{**}_{\mathrm{ground}}$ via vibrational oscillation prior to dissociation (see Fig. 2.2).
2. The rate of dissociation is slow relative to the rate of redistribution of the initial excitation energy over all degrees of freedom.
3. Ions generated in a mass spectrometer represent isolated systems in a series of internal equilibrium.

Thus, a vibrationally excited molecular ion, $\mathrm{A}^{+\bullet\cdot**}$, in the electronic ground state undergoes unimolecular dissociation following the RRKM scheme as described by $k(E)$ in the previous section.

The kinetic energy release (KER) distribution, $P(E, \varepsilon_t)$, via dissociation can be obtained by

$$P(E, \varepsilon_t) = \frac{G(E - E_0 - \varepsilon_t)}{G(E - E_0)} = (s-1)\frac{(E - E_0 - \varepsilon_t)^{s-2}}{(E - E_0)^{s-1}}. \qquad (2.15)$$

Herein, ε_t is the kinetic energy released via dissociation, and $P(E,\ \varepsilon_t)$ is the monotonically decreasing function having its maximum at $\varepsilon_t = 0$.

Then, the averaged KER is obtained as

$$\bar{\varepsilon}_t = \int_0^{E-E_0} \varepsilon_t P(E,\ \varepsilon_t)\ \mathrm{d}\varepsilon_t = \frac{(E-E_0)}{s}. \tag{2.16}$$

Equation (2.16) means that the initial internal excess energy $E - E_0$ is dispersed equally via each possible free motion. Equation (2.16) can be compared with the empirical correlation found by Haney and Franklin for numerous experiments [9]:

$$\bar{\varepsilon}_t = \frac{(E-E_0)}{0.44s} \tag{2.17}$$

in which the denominator $0.44s$ is the parameter called "effective oscillator."

The modern RRKM theory is constructed by linking the statistical unimolecular reaction rate with its transition state, and so is also referred to as "microcanonical transition state theory" in which vibrational-rotational states are taken into account for the reaction:

$$[\mathrm{A}^{+\bullet}]^{*} \xrightarrow{k(E)} [\mathrm{A}^{+\bullet}]^{\ddagger} \longrightarrow \text{Products}. \tag{2.18}$$

The unimolecular dissociation of an activated molecule A^* occurs by passing through the transition state $\mathrm{A}^{\ddagger}$ corresponding to the unique critical configuration leading to products (see Fig. 2.1). Herein, reaction trajectory from A^* to products is assumed to pass a transition state only once.According to classical statistical mechanics, a total flux of trajectories leading to products through the transition state can be described as

$$\begin{aligned}\frac{\mathrm{d}N}{\mathrm{d}t} &= \frac{N\ \int_0^{H=E-E_0} \cdots \int \mathrm{d}q_2 \cdots \mathrm{d}_{3n}\mathrm{d}p_2 \cdots \mathrm{d}q_{3n}}{\int_{H=E} \cdots \int \mathrm{d}p_1 \cdots \mathrm{d}p_{3n}\mathrm{d}p_1 \cdots \mathrm{d}p_{3n}} = \frac{N\ \int_0^{H=E-E_0} \cdots \int \mathrm{d}q_2 \cdots \mathrm{d}_{3n}\mathrm{d}p_2 \cdots \mathrm{d}q_{3n}\ /\ h^{3n}}{\int_{H=E} \cdots \int \mathrm{d}p_1 \cdots \mathrm{d}p_{3n}\mathrm{d}p_1 \cdots \mathrm{d}p_{3n}\ /\ h^{3n}} \\ &= N\frac{G^{\ddagger}(E-E_0)}{hN(E)}.\end{aligned} \tag{2.19}$$

On the other hand, since the total flux can be written as

$$\frac{\mathrm{d}N}{\mathrm{d}t} = k(E)N \tag{2.20}$$

by using the unimolecular rate constant $k(E)$, the microcanonical rate constant of unimolecular reaction is then obtained as follows:

$$k(E) = S\frac{G^{\ddagger}(E-E_0)}{hN(E)},\ \text{or} = S\frac{\int_0^{E-E_0} N^{\ddagger}(\varepsilon)\mathrm{d}\varepsilon}{hN(E)}. \tag{2.21}$$

Here, S denotes the degeneracy of reaction paths.

2.2 Threshold Photoelectron-Photoion Coincidence Mass Spectrometry

The validity of those theories can be examined experimentally by determining how an energy-selected molecular ion undergoes its unimolecular dissociation. Photoelectron-photoion coincidence (PEPICO) mass spectrometry is the most appropriate method for this purpose. PEPICO mass spectrometry is a powerful method for studying dissociation kinetics of gas-phase ions including determination of their thermochemical quantities [10]. PEPICO mass spectrometry was pioneered by Brehm and Eland more than 40 years ago; a fixed energy light source (usually a He (I) lamp) was used and electrons' energy was analyzed via a retarding grid or hemispherical analyzers [11–13]. Stockbauer and Baer introduced the use of continuum vacuum UV light sources, dispersed by a monochromator, to collect ions in coincidence with threshold photoelectrons (TPE) [11–16]. Threshold PEPICO (TPEPICO) mass spectrometry has been developed as the modern approach because of its better electron energy resolution and more readily extractable ions associated with threshold electron detection. In TPEPICO, only zero-energy (ZKE) electrons are selected for coincidence with the photoions, and the ion energy is scanned by varying the photon energy. The combined photon–electron energy resolution of these experiments approaches, and for one of these instruments has already gone beyond, 1 meV (0.1 kJ mol^{-1}):

$$\mathrm{M} + h\nu \rightarrow \mathrm{M}^{+\bullet}(E = h\nu - I_0) + \mathrm{e}^{-}(\mathrm{ZKE}) \tag{2.22}$$

$$\begin{aligned} \mathrm{M}^{+\bullet}(E) &\xrightarrow{k(E-E_0)} \mathrm{F}^{+} + {}^{\bullet}N + \mathrm{KER} \quad \text{or} \\ &\xrightarrow{k(E-E_0)} \mathrm{F}^{+\bullet} + N + \mathrm{KER}. \end{aligned} \tag{2.23}$$

Thus, TPEPICO mass spectrometric studies can provide the following detailed kinetic and thermodynamic information based on dissociation of energy-selected molecular ions [17,18]:

1. Appearance potentials of fragment ions (thermochemical onsets)
2. Breakdown curves (dissociation pathways)
3. Metastable dissociation rates, $k(E)$
4. KERs

A time-of-flight (TOF) mass spectrometer is typically employed with TPEPICO since it is appropriate for the measurement of dissociation rate constants corresponding to slow and metastable decay occurring within field regions, and of kinetic energy releases from the TOF distributions of fragment ions. Figure 2.3 shows a schematic of instrumentation used for TPEPICO experiments, in which both a threshold electron analyzer and TOF mass spectrometer are utilized. A threshold (ZKE) electron and fragment ions produced via a single photoionization event are detected as a coincidence signal. A photoelectron triggers a TOF measurement as the "start"; its "stop" signal is given by a fragment ion. A slow dissociation taking place in the field region (denoted by the pink-colored area in Fig. 2.3a) is reflected in its asymmetric TOF distribution of product ions.

As shown in Fig. 2.3b, true coincidences give TOF peaks although random coincidences result in exponential signal slope in the TOF mass spectrum, which can be minimized by controlling ionization events. A TOF distribution also reflects the kinetic energy release distribution accompanied by dissociation. When an ion is ejected opposite to (⊏) and toward (→) the detector with a larger KER, as indicated in Fig. 2.3a, the former ions reach the detector with a delay due to retardation by the electric field (E_1) and the latter reach it earlier. An example of coincidence TOF mass spectra is

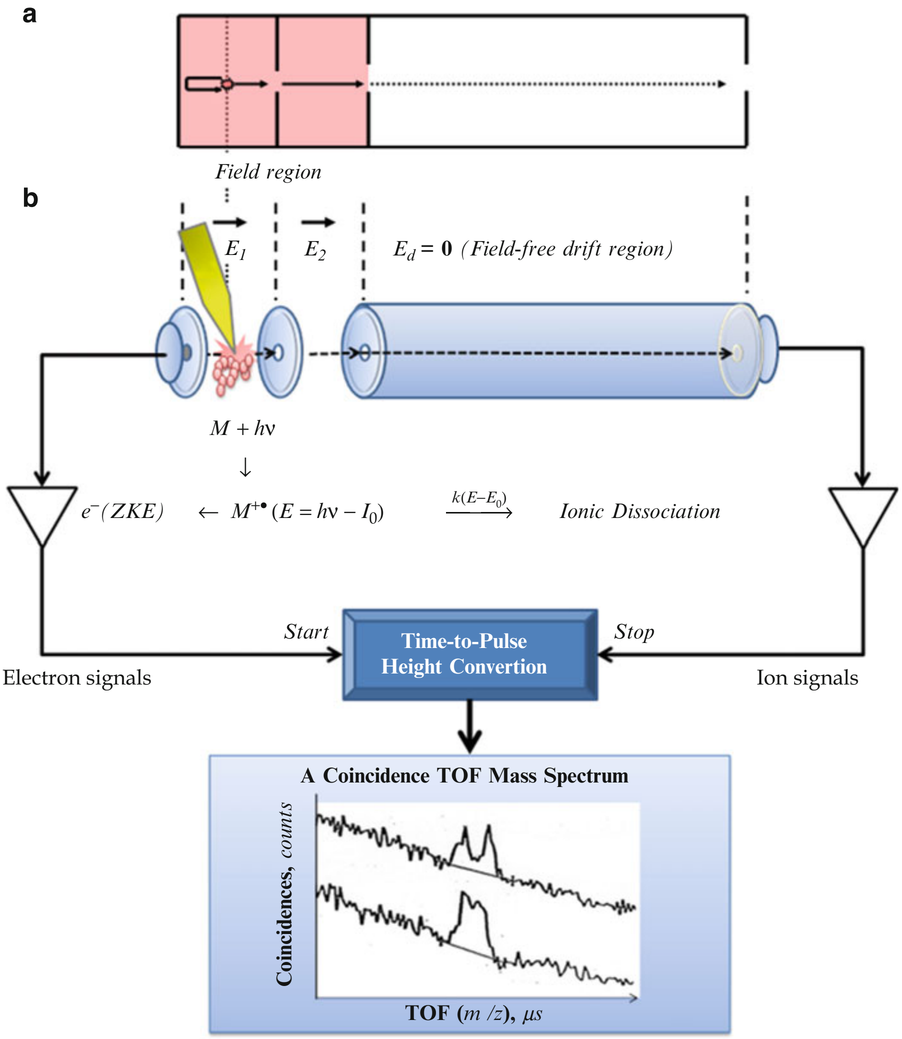

Fig. 2.3 A threshold photoelectron-photoion coincidence (TPEPICO) mass spectrometer equipped with a double-field ionization source

presented in Fig. 2.3b, where a tetrachloromethane ion rapidly decomposes to a trichloromethane ion accompanied by a large and sharp KER (unpublished data):

$$CCl_4^{+\bullet} \rightarrow Cl_3^{+} + {}^{\bullet}Cl + \text{large KER}. \qquad (2.24)$$

The dual-peak-shaped distribution observed in the coincidence TOF mass spectrum of CCl_3^+ in Fig. 2.3b is derived from the presence of defined apertures toward the detector in the ionization source.

2.3 Modeling of Dissociation Dynamics: RRKM and Phase Space Theory

The mass spectrum measured by a mass spectrometer results from an integration of the microcanonical rate constant, $k(E)$, being detected as individual ions via the following factors: (1) the initial excitation energy distribution in ionization; (2) thermal energy distribution of a molecule, P_B, prior to ionization; and (3) the reaction time, τ, specific to an apparatus [19]. When the reactant state is at constant temperature, T, and has the Boltzmann distribution, such a molecular assembly is referred to as a “canonical ensemble” and the canonical rate constant $k(T)$ can be written as

$$k(T) = \int_0^\infty k(E) P_B(E, T)\, \mathrm{d}E, \tag{2.25}$$

where $P_B(E, T)$ is the normalized Boltzmann distribution function. However, in order to study both reaction dynamics mechanisms and the validity of statistical theories the direct measurement of the microcanonical rate constant, $k(E)$, is essential.

Modern theories of unimolecular dissociation can be classified mainly as the tight-transition RRKM model and loose transition phase space (PS) model [20,21]. However, the two types of transitions incorporated in these models can be understood to approximate a real dissociation dynamics on an intrinsically multidimensional potential supersurface along the reaction coordinates.

A schematic of a hypothetical supersurface displaying reaction coordinates is illustrated in Fig. 2.4. The theories of mass spectra, QET, and/or the RRKM model hypothesize an equilibrium between the “activated complex” and “tight” transition state along the reaction coordinates. The “tight” transition state is located as a “hump” on the potential surface determining both dissociation rate and energy dissipation of products. However, it remains difficult to determine the transition state for a specific dissociation reaction. The cases where there is no “hump” along the reaction coordinates are more difficult but the statistical phase space theory (PST) [21] addresses them in terms of the equilibration between the reactant and product states:

$$[A^{+\bullet}]^{**} \longrightarrow [A^{+\bullet}]_{tight} \rightarrow [A^{+\bullet}]_{loose} \longrightarrow Products$$

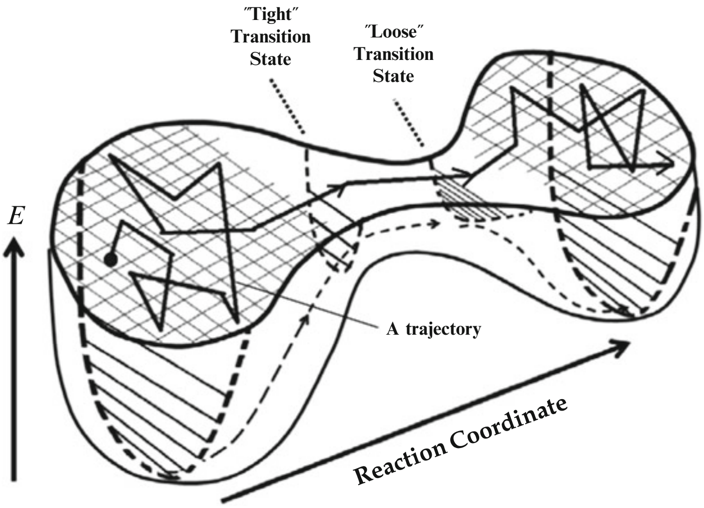

Fig. 2.4 A visualized schematic potential supersurface along a reaction coordinate. The state of a reactant molecular ion proceeds along the reaction coordinate to the states of the product passing through the rate-determining “tight” RRKM transition state and the “loose” PS transition determining the energy partitioning of the product (see [22–24] for fundamental properties of reaction potential surfaces)

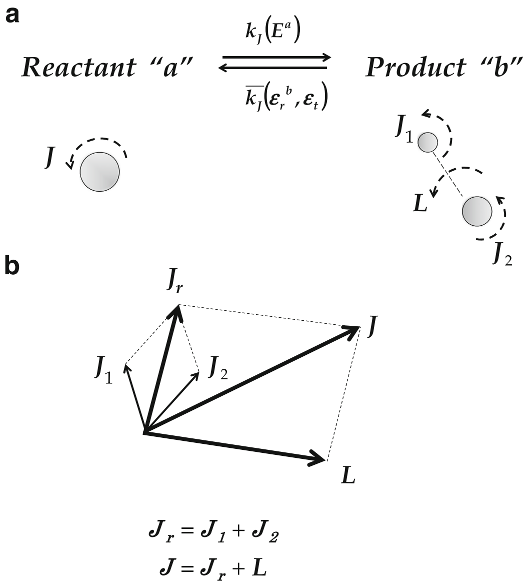

Fig. 2.5 The conservation of total angular momenta and coupling of each momentum. J_1 and J_2 are the rotational angular momentum vectors of products, J_r their total momentum vector, and L the orbital angular momentum vector

Consider a system consisting of the molecular ion as the reactant "*a*" and the product (the fragment ion plus neutrals) "*b*." In PST both the forward and reverse reaction fluxes are in detailed equilibration so that the total angular momentum J and total internal energy E^a are conserved, namely,

$$R_J(a \rightarrow b) = R_J(b \rightarrow a). \tag{2.26}$$

The coupling of angular momentum vectors between "*a*" and "*b*" is shown in Fig. 2.5.

The reverse reaction rate is given by the association reaction rate $\overline{k}_J\ (\varepsilon_r{}^b,\ \varepsilon_t)$ between an ion and neutral species with available relative translational energy ε_t and total rotational energy, $\varepsilon_r{}^b$. Assuming that *Langevin* ion-molecular reaction model [25] is applied to this association reaction, there is no need for activation energy. The only reaction barrier is the local maximum point of the effective potential that consists of long-range ion-dipole potential and centrifugal force between an ion and neutral species, and an association reaction takes place whenever the energetics of a projectile ion and neutral molecules equal or exceed the maximum of this potential barrier. Therefore, the transition state in PST is often termed an "Orbiting" transition state since it is defined as this maximum point along the association reaction [21].

A cautionary note is in order regarding the proper use of RRKM calculations. The RRKM theoretical frame calculations compare only the properties of the transition state of the fragmenting molecule ($A^{\ddagger}$) with those of the excited normal configuration of the molecule (A^*). Therefore RRKM theory is only appropriate for calculating rates or state distributions in the region of the transition state on the potential surface. RRKM theory is not appropriate for calculating properties of the system in the product region of the energy surface. Other simplifying assumptions should be kept in mind as well. There are $3n - 12$ vibrational degrees of freedom in the products versus $3n - 6$ in the normal configuration of the fragmenting molecule and $3n - 7$ in the transition state. This situation is not considered in RRKM analysis. Also in the classical RRKM theory neither conservation of angular momentum nor long-range potential of the system are taken into account.

The microcanonical dissociation rate constant of the reactant “*a*” with rotational angular momentum J can be expressed as

$$k_J(E^a) = \frac{\sigma_a S_r{}^b}{\sigma_b S_r{}^a} \left\{ \frac{\iint \overline{k_J}(\varepsilon_r{}^b,\ \varepsilon_t) N_t(\varepsilon_t) N_r(\varepsilon_r{}^b) \mathrm{d}\varepsilon_t\, N_b(E^a - E_0 - \varepsilon_{tr}{}^b) \mathrm{d}\varepsilon_{tr}{}^b}{N^a(E^a - \varepsilon_r{}^a)} \right\}. \tag{2.27}$$

Herein, $N_t(\varepsilon_t)$, $N_r(\varepsilon_r{}^b)$, and $N_b(E^a - E_0 - \varepsilon_{tr}{}^b)$ are, respectively, the state densities of translation, rotation, and vibration of the product “*b*”. $S_r{}^a$ and $S_r{}^b$ are degeneracies of spatial angular momenta of the system “*a*” and “*b*.” σ_a and σ_b are the numbers of symmetry for the forward $a \rightarrow b$ and reverse $b \rightarrow a$ reactions. Then, the rate constant to be compared to experiment can be obtained by averaging the thermal distribution $P(J)$ of J:

$$k(E^b) = \frac{\int_0^\infty k_J(E^b) P_J(J)\, \mathrm{d}J}{\int_0^\infty P_J(J)\, \mathrm{d}J}. \tag{2.28}$$

The probability that the reactant “*a*” decomposes with internal energy E^a and angular momentum J, and accompanying KER ε_t, is given as

$$P_J(E^a,\ \varepsilon_t) = \frac{k_J(E^a,\ \varepsilon_t)}{k_J(\varepsilon_t)}. \tag{2.29}$$

Dissociations can be only observed when an ion decomposes within the field region in a TOF mass spectrometer (shown in Fig. 2.3a). In general this time window is defined between an entering time τ_1 and exiting time τ_2. The probability that the reactant “*a*” decomposes between τ_1 and τ_2 becomes

$$P_\tau(E^a, J) = \exp\{-k_J(E^a)\tau_1\} \quad - \exp\{-k_J(E^a)\tau_2\}, \tag{2.30}$$

whereas τ_1 is usually 0 in a TOF mass spectrometer. Therefore, the KER distribution obtained from TPEPICO experiments is described as

$$P(\varepsilon_t) = \frac{\int_0^\infty \mathrm{d}J\ P(J) P_\tau(E^a,\ J)\ P_J(E^a,\ \varepsilon_t)}{\int_0^\infty \mathrm{d}J\ P(J) P_\tau(E^a, J)} \tag{2.31}$$

and the averaged KER ($\overline{\varepsilon_t}$) at a given E^b will be

$$\overline{\varepsilon_t}(E^b) = \frac{\int_0^{E^b} \varepsilon_t P(\varepsilon_t) \mathrm{d}\varepsilon_t}{\int_0^{E^b} P(\varepsilon_t) \mathrm{d}\varepsilon_t}. \tag{2.32}$$

As an example, the dissociation rates and averaged KERs for the formation of phenyl cation from nitrobenzene radical cation [26]

$$\mathrm{C_6H_5 - NO_2{}^{+\bullet} \rightarrow C_6H_5{}^{+} + NO_2{}^{\bullet}} \tag{2.33}$$

are shown in Fig. 2.6.

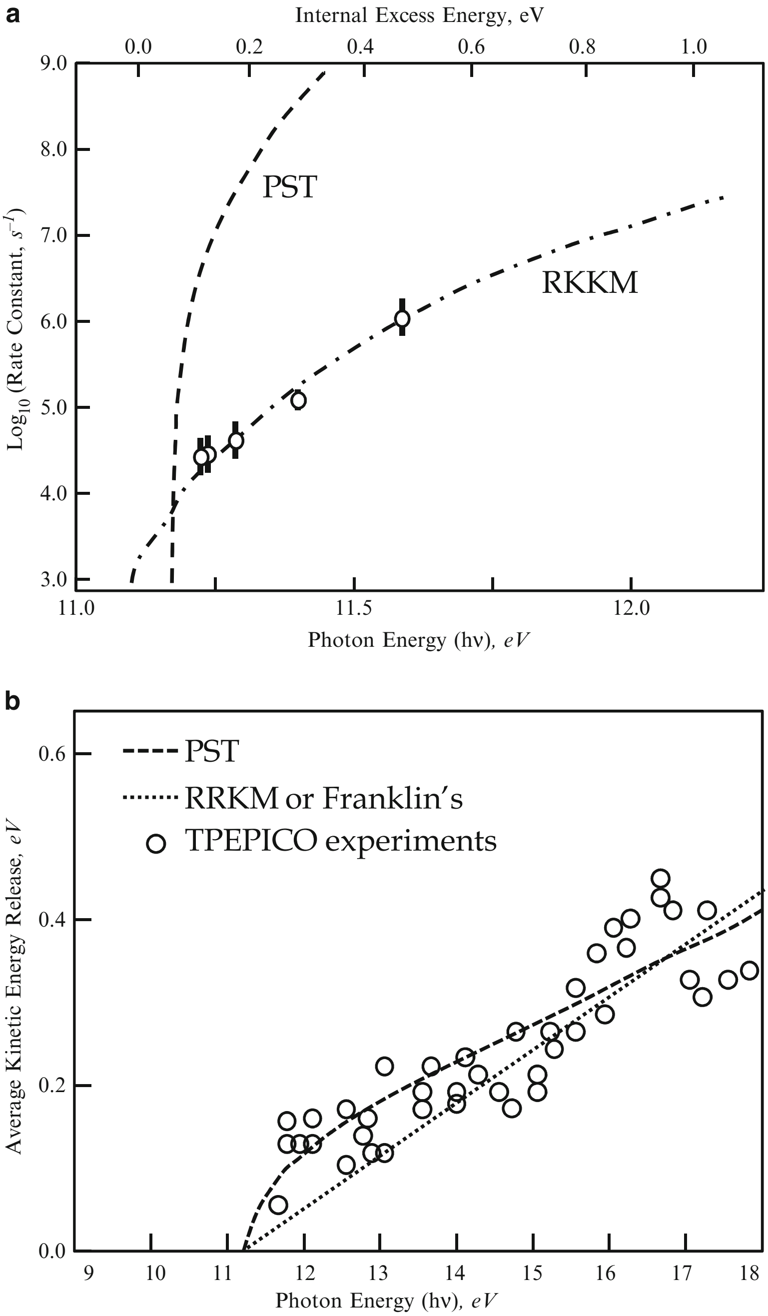

Fig. 2.6 (**a**) The dissociation rate constants and (**b**) kinetic energy releases in the dissociation of $C_6H_5NO_2^{+\bullet}$ to $C_6H_5^+$ and $NO_2^{\bullet}$, measured by the TPEPICO experiments [26] (those figures newly redrawn)

The TPEPICO decay rates (ϕ) as a function of internal excess energy were well interpreted by the RRKM calculation whereas the PST predicted much higher rates. In contrast, the averaged KERs obtained experimentally seem to be better fitted with PST although both PST and Franklin's empirical formulae gave reasonable matches to experiment. Even in the case where a potential surface is smooth without the "rigid" transition state (which is the model of the RRKM tight transition state, the so-called hump) from the reactant “*a*” to the product “*b*,” the rate-determining factor is the RRKM decay rate corresponding to the lowest density state perpendicular to the reaction coordinate. The “Orbital” transition state is located much closer to the product “*b*,” and so their energy partitioning including kinetic energy release is determined. Therefore, several transition states along the reaction coordinates are utilized to approximate a real reaction dynamics of dissociation. In Fig. 2.4, a rigid RRKM transition state and loose “Orbital” transition state are indicated along the reaction supersurface. As seen in the example of the phenyl cation formation from the nitrobenzene radical cation, the rate constant is supposed to fit the RRKM theory since the reaction flux of the RRKM transition state is rate limiting while the KER reflecting the final energy partitioning would be determined by the “Orbiting” state. This concept was first introduced by Miller (1976) [27] as the unified statistical theory (UST), in which at least two “transition states” are assumed on the reaction coordinate.

2.4 Breakdown Curves

The validity of statistical theories can be assessed in their comparison with experimentally constructed breakdown curves for the molecular ion and its product ions. Experimental breakdown curves are obtained by TPEPICO mass spectra measured as a function of photon energy. Breakdown curves are the plot of product-ion relative abundances with a certain reaction time contingent on the internal energy of the molecular ion. With a known internal energy distribution of the molecular ion $P_{\mathrm{int}}(E)$ resulting from ionization, the relative abundance of a product ion $[\mathrm{m}^+]_t$ at a reaction time t can be given as

$$[\mathrm{m}^+]_t = \int_0^{E_{\max}} P_{\mathrm{int}}(E) B_{m^+}(E,\, t)\mathrm{d}E, \tag{2.34}$$

where $B_{\mathrm{m}^+}(E,\, t)$ is the breakdown curve of the product ion m^+. The reaction time is that required for a molecular ion to travel across the field regions ($\vec{E}_1$ and $\vec{E}_2$ in Fig. 2.3).

2.4.1 Consecutive Reaction

For the following consecutive reaction

$$\mathrm{A}^+ \xrightarrow{k_1(E)} \mathrm{m}_1^+ \xrightarrow{k_2(E)} \mathrm{m}_2^+, \tag{2.35}$$

the relative abundances of product ions at the reaction time t as a function of the internal energy E are given by

$$\begin{aligned}
[\mathrm{A}^+]_t &= \exp(-k_1 t) \\
[\mathrm{m}_1^+]_t &= k_1 \frac{\{\exp(-k_1 t) - \exp(-k_2 t)\}}{k_2 - k_1} \\
[\mathrm{m}_2^+]_t &= 1 - \frac{\{k_2 \exp(-k_1 t) - k_1 \exp(-k_2 t)\}}{k_2 - k_1}
\end{aligned} \tag{2.36}$$

and herein $[\mathrm{A}^+]_{t=0} = 1$.

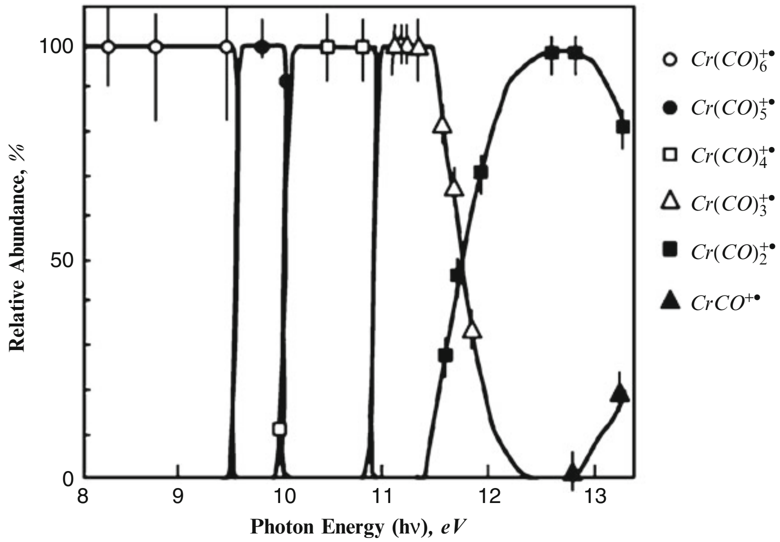

Fig. 2.7 The TPEPICO breakdown curves of hexacarbonyl chromium ion (modified from [28])

A typical consecutive reaction can be found in the dissociation of hexacarbonyl chromium ion, $\mathrm{Cr(CO)_6^{+\bullet}}$ [28]. The experimentally elucidated breakdown curve of this molecular ion reflects its consecutive fragmentations with the successive loss of CO up to the photon energy less than 13 eV (Fig. 2.7):

$$\begin{aligned}\mathrm{Cr(CO)_6^{+\bullet}} &\xrightarrow{-\mathrm{CO}} \mathrm{Cr(CO)_5^{+\bullet}} \xrightarrow{-\mathrm{CO}} \mathrm{Cr(CO)_4^{+\bullet}} \\ &\xrightarrow{-\mathrm{CO}} \mathrm{Cr(CO)_3^{+\bullet}} \xrightarrow{-\mathrm{CO}} \mathrm{Cr(CO)_2^{+\bullet}}.\end{aligned} \tag{2.37}$$

As a different example, it has been known that $\mathrm{C_{60}^{+\bullet}}$ undergoes successive loss of $\mathrm{C_2}$ up to the molecular internal energy less than 80 eV (Fig. 2.8) [29]. With increasing internal energy, the fullerene radical cation changes its 3-D structure, from the so-called Solid to Floppy phase and from Floppy to Pretzel phase. Moreover, the fullerene radical cation explosively dissociates to the small carbon-cluster ions at the same internal energy which coincided with the internal energy equal to the Pretzel phase (Fig. 2.9). This dissociative behavior of $\mathrm{C_{60}^{+\bullet}}$ has been observed from the relative cross-section measurements for the collision-induced dissociation of $\mathrm{C_{60}^{+\bullet}}$ by varying the center-of-mass (CM) collision energy in mass-analyzed ion kinetic energy spectroscopy (MIKES) experiments.

2.4.2 Competitive Reaction

Similarly, for the simple competitive reaction

$$\begin{tikzcd}
 & {[m_1^+]} \\
{[A^+]} \arrow[ur, "k_1(E)"] \arrow[r, "k_2(E)"] \arrow[dr, "k_3(E)"'] & {[m_2^+]} \\
 & {[m_3^+]}
\end{tikzcd} \tag{2.38}$$

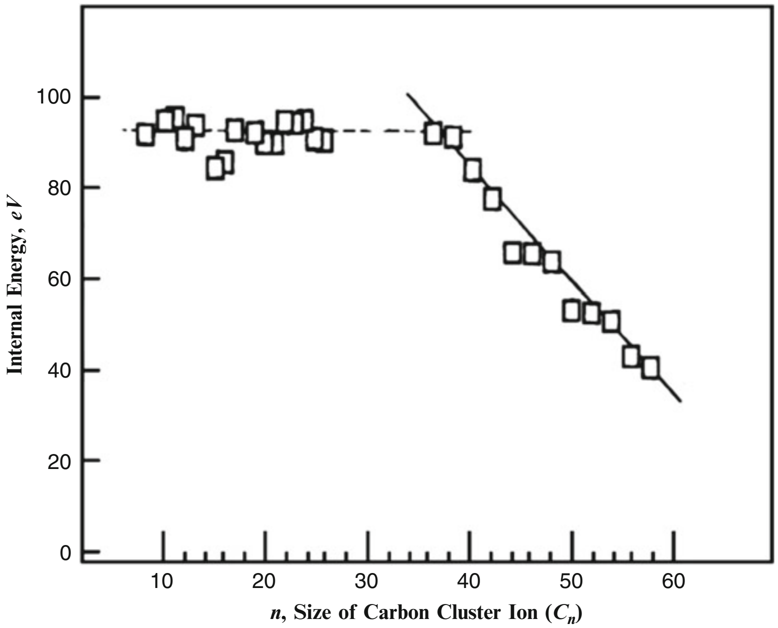

Fig. 2.8 Appearance energies of carbon-cluster ions elucidated from the CM collision energy-dependent MIKES experiments (modified from [29])

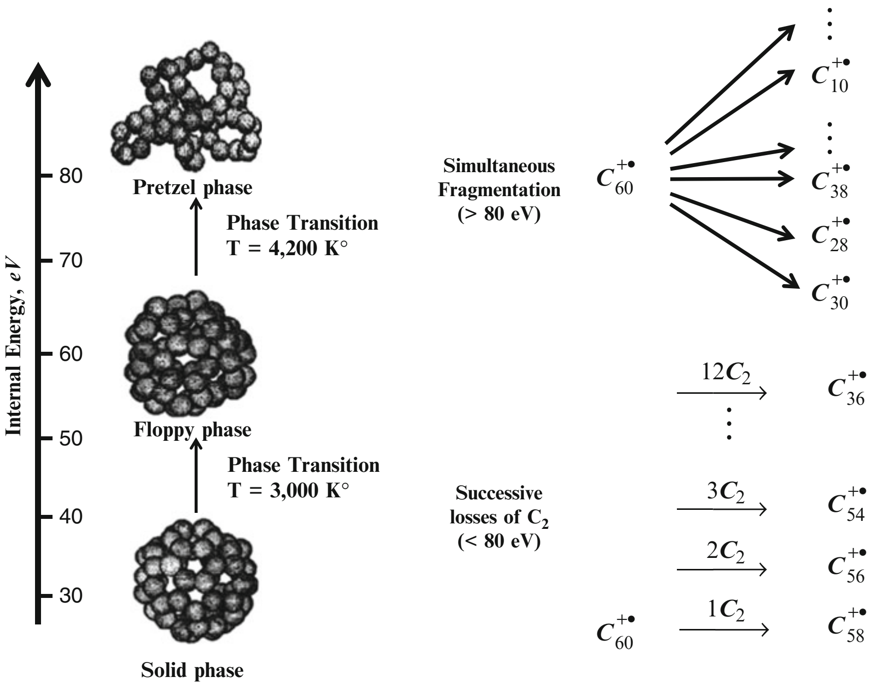

Fig. 2.9 The successive fragmentation of the fullerene radical cations $C_{60}^{+\bullet}$ occurring at lower internal energies, and their fragmentations to the smaller carbon-cluster ions simultaneously at the Pretzel phase

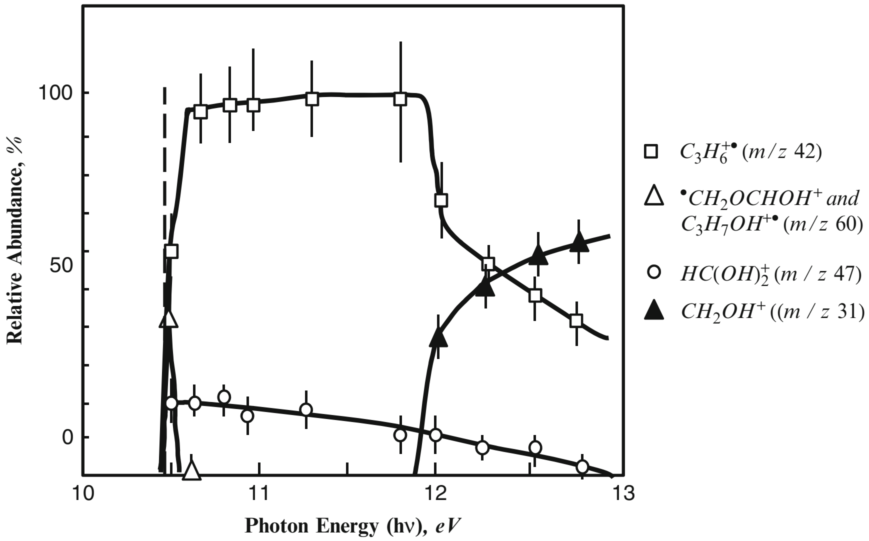

Fig. 2.10 The TPEPICO breakdown curves of propyl formate radical cation at a photon energy of 10–13 eV (modified from [30])

the relative abundance of their product ions at the reaction time t as a function of E is

$$\begin{aligned}
&[\mathrm{A}^+]_t = \exp(-k_{\mathrm{total}}\, t) \\
&[\mathrm{m}_i^+]_t = k_i \frac{\{1 - \exp(-k_{\mathrm{total}}\, t)\}}{k_{\mathrm{total}}} \quad (i = 1,\, 2, 3).
\end{aligned} \tag{2.39}$$

Here, k_{total} is the total reaction rate constant $(= k_1 + k_2 + k_3)$. Their breakdown curves are given merely as the ratio among respective reaction rate constants.

Breakdown curves can determine the appearance potentials (APs) of fragment ions and give the possible fragmentation scheme of a molecular ion. Such direct comparison with statistical theories can provide insight into ionic dissociation dynamics.

The following breakdown curves are obtained for propyl formate radical cations, $HCOOC_3H_7^{+\bullet}$, by using TPEPICO mass spectrometry (the energy resolution of threshold photoelectrons is ca. 21 meV) [30]. Of particular significance in this breakdown curves is that the appearance energies of four fragment ions $C_3H_6^{+\bullet}$ (*m*/*z* 42), $HC(OH)_2^+$ (*m*/*z* 47), and $^{\bullet}CH_2OCHOH^+$ and $C_3H_7OH^{+\bullet}$ (*m*/*z* 60) are identical with the measured ionization energy of the propyl formate molecule (that is, 10.45 ± 0.05 eV as indicated by the dashed line in Fig. 2.10). These observations are interpreted by assuming that the propyl formate radical cation first isomerizes to the distonic intermediate (*i*) prior to dissociation, and then competitive fragmentations occur via this distonic intermediate (Fig. 2.11). A possible mechanism for the formation of $C_3H_6^{+\bullet}$ (*m*/*z* 42) is a two-step McLafferty rearrangement (Fig. 2.12), involving the intermediacy of a distonic radical cation (*i*). The formation of $HC(OH)_2^+$ is the so-called [R–2H] loss reaction or "McLafferty +1" rearrangement. Both occur via the intermediacy of (*i*).

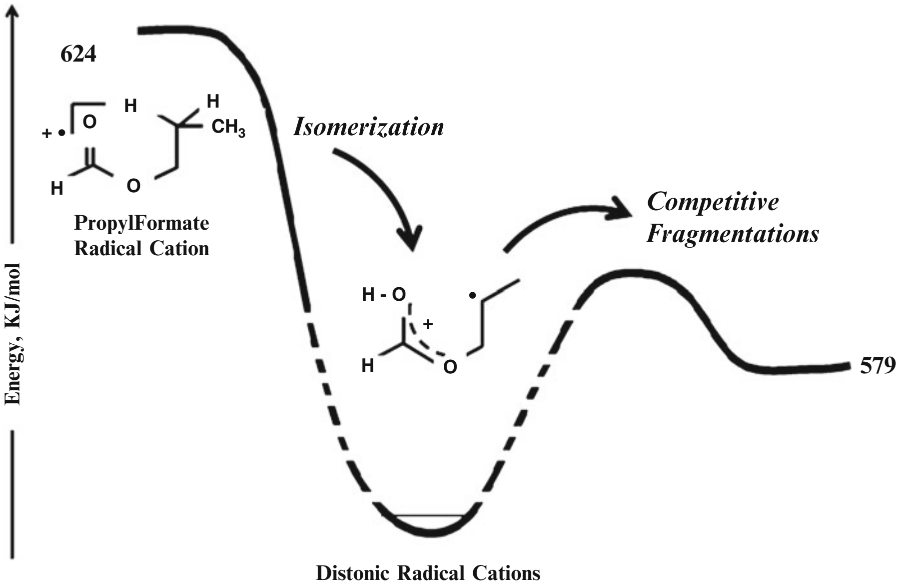

Fig. 2.11 A schematic potential energy surface for the fragmentation of the propyl formate radical cation undergoing isomerization to a distonic radical cation (*i*)

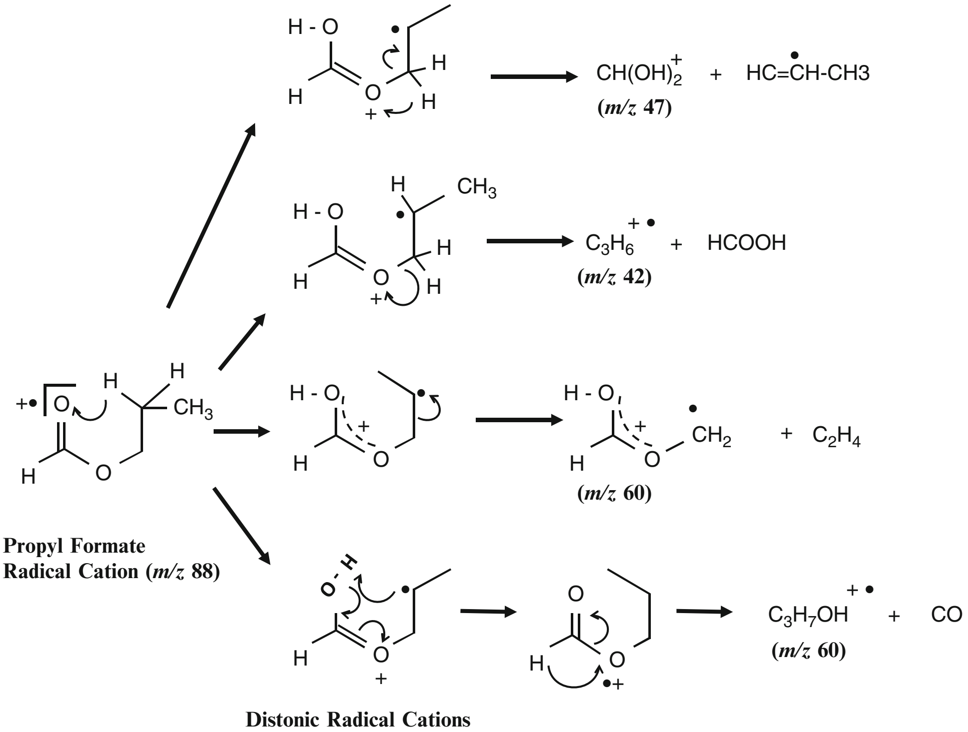

Fig. 2.12 Competitive fragmentations from a distonic radical cation that is formed via *MacLafferty* rearrangement of the propyl formate radical cation prior to dissociation

2.5 TOF Distributions of Product Ions

The TOF distribution of a product ion would reflect both the dissociation rate $k(E)$ and KER in dissociation.

2.5.1 Metastable Dissociations

Metastable dissociations occurring in the field regions (indicated in pink in Fig. 2.13 and also in Fig. 2.3a) result in asymmetric TOF distributions of product ions whereas for dissociation in the field-free drift region the TOF of its product ions is the same as that of the molecular ion. Figure 2.13 illustrates the origin of asymmetric TOF distribution of product ions.

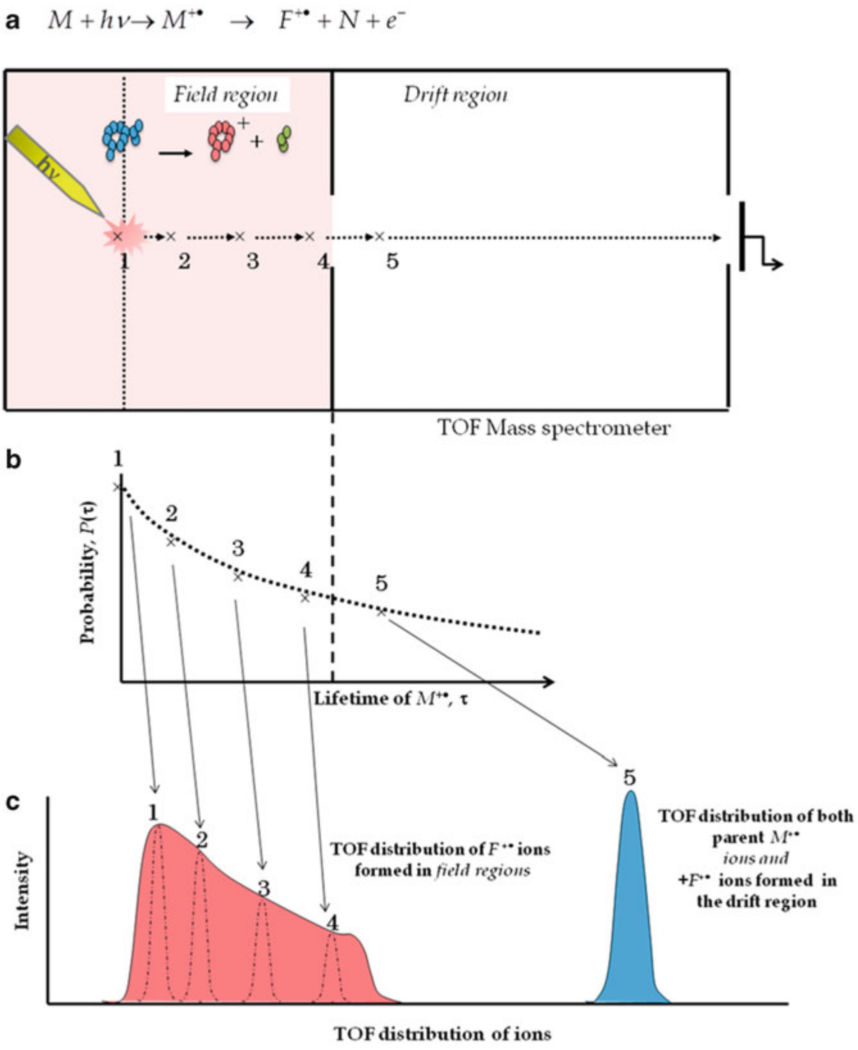

Fig. 2.13 Metastable dissociation of a parent ion ($M^{+\bullet}$) to a product ion ($F^{+\bullet}$) and their TOF distributions

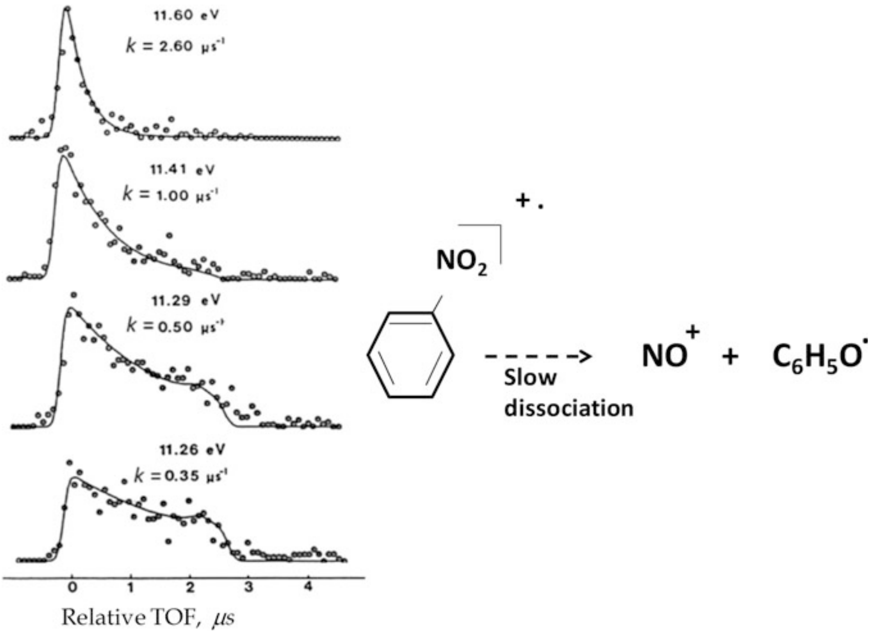

Fig. 2.14 Asymmetric TOF distributions due to metastable fragmentation (modified from [26]). The metastable formation of NO^+ from nitrobenzene radical cation. Individual dissociation rates (k) were obtained so that TOF distributions could be obtained on the basis of ion trajectory calculation assuming that lifetimes of the parent ion (*solid curves*) give the best fit to experiments (*filled circle*)

Figure 2.14 shows the examples of asymmetric TOF distributions due to metastable decay occurring in the electric field regions. Based on ion trajectory calculations, metastable decay constants can be elucidated from the best least-square fit curve with experimental TOF distributions.

2.5.2 Kinetic Energy Releases in Dissociation

When the isotropic fragmentation of the ion M^+ to the fragment ion m^+ and neutral fragment $[M - m]$ accompanies a single KER Q_i in center of mass

$$M^+ \rightarrow m^+ + [M - m] + Q_i \tag{2.40}$$

the TOF distribution $F(\tau;\ Q_i)$ of the ion m^+ can be calculated numerically. Each TOF distribution observed, $F(\tau)$, is deconvoluted by a set of the TOF distributions $F(\tau;\ Q_i)$ corresponding to a series of KERs defined as

$$Q_i = (2i - 1)^2 E_0. \tag{2.41}$$

Herein, $F(\tau;\ Q_i)$ is normalized and E_0 is chosen as the minimum KER to broaden a thermal peak by one channel width of a TOF spectrum. Then, from the coefficients $W(i)$ which give the best fit to experiment

$$F(\tau) = \sum_i W(i) F(\tau; Q_i). \tag{2.42}$$

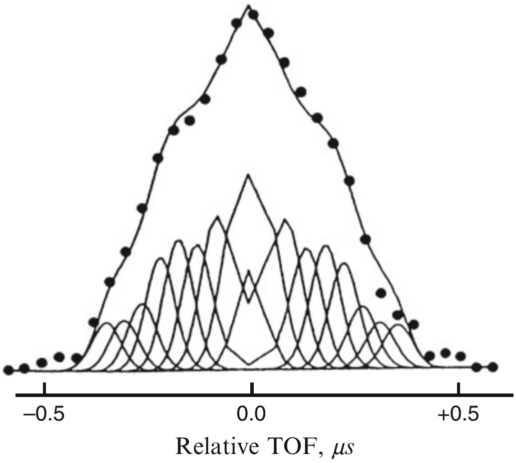

Fig. 2.15 A TPEPICO TOF distribution of *m*/*z* 29 ion produced from $\mathrm{HCOOH}^{+\bullet}$ at the photon energy of 7.28 eV. Using $E_0 = 8.16$ meV and room temperature $T = 300$ K°, the experimental $F(\tau)$ (*filled circle*) was deconvoluted with the calculated $F(\tau;\ Q_i)$ with the nine discrete KERs $Q_i(i = 1 - 9)$ (*solid curves*) (modified from [31])

The KER distribution (KERD), $P(Q_i)$, can be formulated as

$$P(Q_i) = \frac{\left[\frac{W(i)}{\sum_i W(i)}\right]}{[4(2n-1)E_0]}. \tag{2.43}$$

The averaged KER can then be given as

$$\langle Q \rangle = \frac{\sum_{i=1}^{l} Q_i P(Q_i)}{\sum_{i=1}^{l} P(Q_i)}. \tag{2.44}$$

Figure 2.15 shows the TOF distribution of *m*/*z* 29 ion obtained by TPEPICO experiments of the formic acid radical cation [31]:

$$\mathrm{HCOOH} \xrightarrow{17.28\,\mathrm{eV}} [m/z\ 29]^{+} + {}^{\bullet}\mathrm{OH} + \mathrm{e}^{-}. \tag{2.45}$$

2.6 Energy Disposal and Theoretical Expectations

The theoretical model commonly used to describe the KERD is based on statistical theory, in which the energy in excess of the dissociation limit is assumed to be distributed statistically among the product electronic, vibrational, rotational, and translational degrees of freedom, subject only to the conservation of angular momentum. The average energy deposited in the various modes can be easily calculated by

$$E^{*} = \langle E_t \rangle + \langle E_r \rangle + \langle E_v \rangle, \tag{2.46}$$

in which E^* is the energy in excess of the dissociation limit, and $\langle E_t \rangle$, $\langle E_r \rangle$, and $\langle E_v \rangle$ are, respectively, the average energies residing in the translational, rotational, and vibrational degrees of freedom. To assess how experiments compare with theoretical expectations, there are several approaches described below.

2.6.1 Scaling Law

The scaling law was first applied to thermodynamics of phase transition by Widoim [32] and Domb and Hunter [33]. The function Γ is defined to be homogeneous when Γ has the following relation with the scaling λ:

$$\Gamma(\lambda r) = \lambda^p \Gamma(r). \tag{2.47}$$

Herein, p is the degree of homogeneity. In cases where Γ has two variables, r and q, it can be similarly expressed as

$$\Gamma(\lambda r, \lambda q) = \lambda^p \Gamma(r, q). \tag{2.48}$$

Then, by defining $\lambda = 1/r$ (2.48) can be rewritten as

$$\Gamma\left(1, \frac{q}{r}\right) = r^{-p} \Gamma(r, q). \tag{2.49}$$

This means that by conversions with $q \;\rightarrow q/r$ and $\Gamma \rightarrow r^{-p}\Gamma$, all points $(r; \Gamma(r, q))$ are located on one smooth curve being determined by only one variable q/r.

When this scaling law is applied to the kinetic energy distribution $P(E, \varepsilon_t)$, this distribution as a function of different internal energy E will be plotted on one distribution if $P(E, \varepsilon_t)$ is homogeneous as per the following conversion:

$$\begin{aligned} \varepsilon_t &\rightarrow \frac{\varepsilon_t}{E} \\ P &\rightarrow EP. \end{aligned} \tag{2.50}$$

It can be demonstrated that the KERD based on RRKM theory is expressed by a single curve by the above conversion. For an example, the classical RRKM KERD is given by

$$\begin{aligned} P(E^a, \varepsilon_t) &= \frac{N^{\ddot{o}}(E^a, \varepsilon_t)}{G^{\ddot{o}}(E^a)} \\ &= s\,\frac{(E^a - \varepsilon_t)^{s-1}}{(E^a)^s} = s\left(\frac{E^a - \varepsilon_t}{E^a}\right)^{s-1} \frac{1}{E^a}. \end{aligned} \tag{2.51}$$

Therefore, the conversion results in

$$E^a P(E^a, \varepsilon_t) = s\left(1 - \frac{\varepsilon_t}{E^a}\right)^{s-1}. \tag{2.52}$$

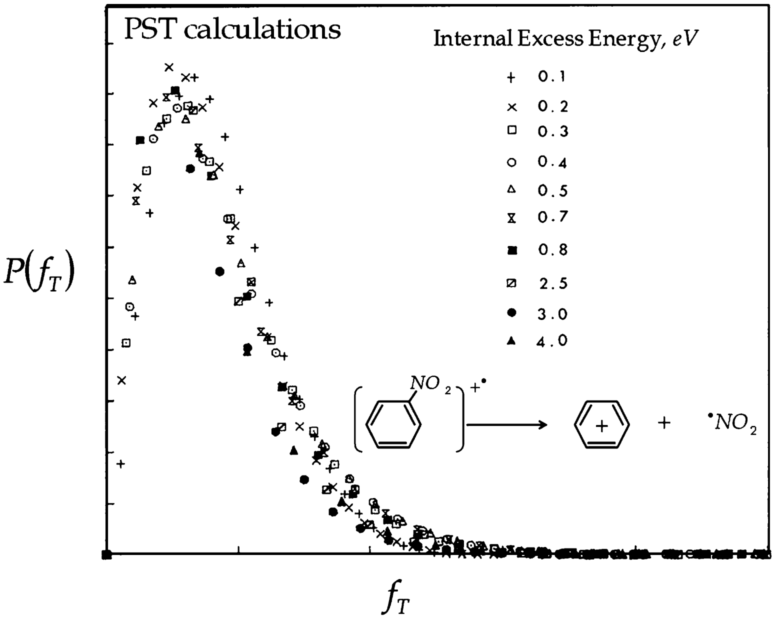

Fig. 2.16 The scaling plots of KERDs for the dissociation of nitrobenzene ion $C_6H_5NO_2^{+\bullet}$ to phenyl cation $C_6H_5^+$ and $^\bullet NO_2$, calculated at various internal excess energies by PST

That is, for the one variable $f_T = \varepsilon_t/E^a$, $P(f_T) = E^a P(E^a, \varepsilon_t)$ becomes the single distribution. This is a central feature of statistical theories in which the internal excess energy is uniformly distributed to all available degrees of freedom regardless of its value. This applies to the statistical phase space (PS) theory. Figure 2.16 shows the KERD calculated by PST and obtained by the conversion (2.52) for the dissociation of nitrobenzene molecular ion to phenyl cation (unpublished data).

In the TPEPICO experiments of ethyl bromide ions ($C_2H_5Br^{+\bullet}$) [34], the KERDs for the formation of $C_2H_5^+$ were extracted as a function of the parent-ion internal energy as described in the previous section. Those KERDs were converted using $f_T = \varepsilon_t/E^a$ and $P(f_T) = E^a P(E^a, \varepsilon_t)$ as plotted in Fig. 2.17. If all fragmentations to $C_2H_5^+$ occur in the same dynamic range, then the scaling plot of KERDs should be represented by a single curve. However, Fig. 2.17 features two different curves in the scaling plot of KERDs. That is, the KERDs for the ethyl bromide ion dissociation were statistical only in the region of the ground electronic state. Ions prepared in the A state have KERDs characteristic of a direct dissociation. This indicates that the direct dissociation rate is faster than the rate of radiationless transition to the ground electronic state. The QET assumes that the internal conversion of the initially excited electronic states to the ground state takes place much faster than ionic dissociation. The scaling plot for the formation of $C_2H_5^+$ from $C_2H_5Br^{+\bullet}$ [34] represents an example of a breakdown of the QET.

2.6.2 Information Theoretical Approach

Another approach to examine how the state distribution of products resulting from the reactant matches theories is based on information theory. Jaynes [35] first presented a mathematical link to statistical mechanics with the information theory, which Levine and Bernstein then applied to molecular reaction dynamics [36,37]. The central concerns are (1) "What is the prior expectation?" and "What is the measure for deviation from expectation?" To answer these questions, the "Surprisal" concept was introduced.

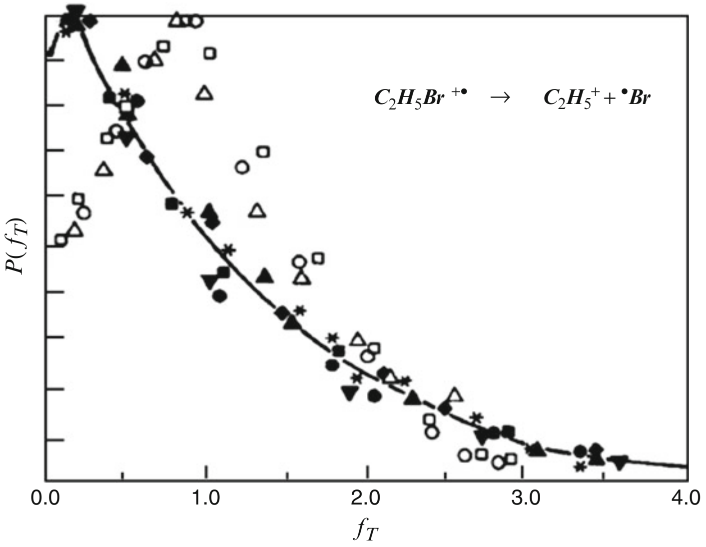

Fig. 2.17 The scaling plots of KERDs for the dissociation of ethyl bromide $C_2H_5Br^{+\bullet}$ to $C_2H_5^{+}$ and ${}^{\bullet}$Br, revealing a distinct difference between ions with photon energies above (*open circle*, *open triangle*, *open square*) and below (*filled square*, *filled circle*, *filled triangle*, *asterisk*, *inverted triangle*) the Ã state onset near 12.0 eV (modified from [34]). The *solid line* is the result calculated by statistical theory with angular momentum conservation similar to PST

2.6.2.1 Surprisal Analysis

Consider events A, B, etc. which are independent of each other. Each surprisal $I(\mathrm{A})$ is defined as

$$I(\mathrm{A}) \equiv -\ln P(\mathrm{A}). \tag{2.53}$$

Herein, $P(\mathrm{A})$ is the probability of event A. Then the surprisals, $I(\mathrm{A})$ and $I(\mathrm{B})$, satisfy the following mathematical relationship. Since for the probability of event $\mathrm{A} \cap \mathrm{B}$ (“B takes place following A”)

$$P(\mathrm{A} \cap \mathrm{B}) = P(\mathrm{A}) \times P(\mathrm{B}), \tag{2.54}$$

the following relation between surprisals holds:

$$I(\mathrm{A} \cap \mathrm{B}) = I(\mathrm{A}) + I(\mathrm{B}). \tag{2.55}$$

When a priori probability $P^{\circ}(\mathrm{A})$ is given, the surprisal is redefined to be

$$I(\mathrm{A}) \equiv -\ln P(\mathrm{A}) - \{-\ln P^{\circ}(\mathrm{A})\} = -\ln[P(\mathrm{A})/P^{\circ}(\mathrm{A})]. \tag{2.56}$$

In other words, $I(\mathrm{A})$ is the measure for deviation of observed probability $P(\mathrm{A})$ from $P^{\circ}(\mathrm{A})$. The kinetic energy distribution (KERD) is one of physical observations reflecting the energy disposal among final products resulting from dissociation dynamics. A priori KERD would be given by the expectation based on RRKM/PST.

Those surprisal plots clarify deviations from expected values as a function of each state variable (f) of products. Usually, the function

$$P(f)\ /P^{\circ}(f) \equiv \omega(f) \tag{2.57}$$

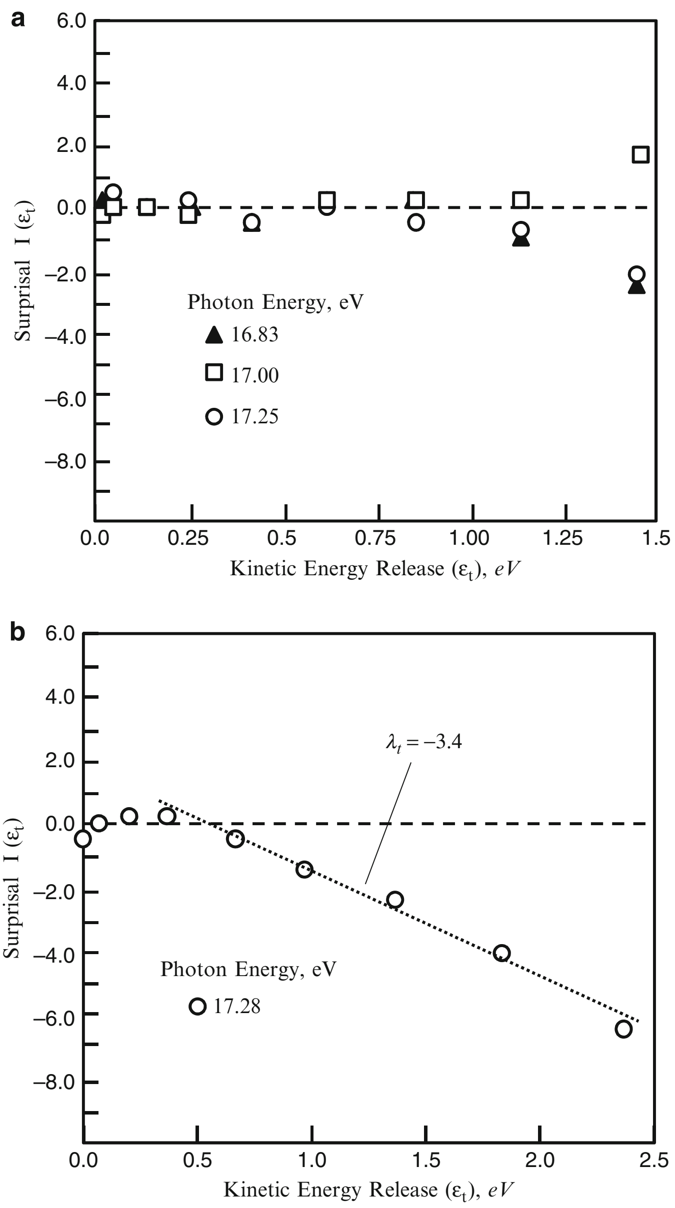

Fig. 2.18 The surprisal plots on KERDs: (**a**) The C_2H_2-elimination from fluorobenzene ion at several photon energies (modified from [38]), and (**b**) the *m*/*z* 29 ion formation from formic acid radical cation $HCOOH^{+\bullet}$ (modified from [31])

is a smooth function. The so-called temperature constant (λ_f) is introduced in relation to each state quantity (vibration, rotation, and translation) to indicate deviation from an expected distribution.

Figure 2.18 shows examples of surprisal analyses on the KERDs observed for two dissociative reactions. The surprisal analysis of KERDs for the C_2H_2-elimination from the fluorobenzene radical cation demonstrates that $I(\varepsilon_t) \approx 0$ over KERs (ε_t) at several photon energies (Fig. 2.18a) [38]. This means that this fragmentation can be interpreted by the statistical RRKM theory. In contrast, the formation of CHO^+ (*m*/*z* 29) from formic acid radical cation showed $I(\varepsilon_t) \approx 0$ with kinetic energies less than 0.5 eV but a surprisal with the linearity ($\lambda_t = -3.4$) was revealed (Fig. 2.18b) [31], most probably indicating participation of two different dissociation dynamics rather than the formation of two different ion species, HCO^+ and COH^+.

Since the slope of the surprisal plot is given by

$$\lambda_f \equiv \frac{\mathrm{d}I(f)}{\mathrm{d}f}, \tag{2.58}$$

an observed distribution $P(f)$ can be expressed with the distribution characterized by λ_f

$$P(f) = P^{\circ}(f)\ \frac{\exp(-\lambda_f f)}{\exp(-\lambda_0)}. \tag{2.59}$$

Herein the denominator is

$$\exp(-\lambda_0) = \sum_f P^{\circ}(f)\exp(-\lambda_f f) \equiv Q_f, \tag{2.60}$$

which serves as the partition function Q_f. That is, the average $\langle f \rangle$ is expressed as

$$\langle f \rangle = \sum_f f\,P(f) = -\frac{\mathrm{d}\ \ln Q_f}{\mathrm{d}\lambda_f}. \tag{2.61}$$

2.6.2.2 Principle of Maximum Entropy [36]

The 1st-order ("linear") surprisal observations can be accounted for by the principle of maximum entropy that follows from statistical dynamics. That is, the most probable distribution being observed is that which has the maximum entropy, subject to the particular constraints of a system. For example, regarding the vibrational state distribution P^v, this system at least is constrained per

$$1 = \sum_j P^v(j) \quad \text{(Normalization)}, \tag{2.62}$$

and

$$\langle E_j^v \rangle = \sum_j P^v(j)E_j^v \qquad \text{(1st momentum term of vibrational energy)}. \tag{2.63}$$

Maximizing the system entropy under the above conditions does correspond to minimizing the "information quantity" (I)

$$I = \sum_j P^v(j)\ln\left[\frac{P^v(j)}{P^{\circ}(j)}\right] \tag{2.64}$$

upon the averaged surprisal (P^v). Then, for its *Lagrangian* (L)

$$L = I + \alpha\langle 1 \rangle + \beta\langle E_j^{\nu} \rangle \tag{2.65}$$

$\delta L = 0$ should be calculated. That is,

$$\begin{aligned} 0 = \delta L &= \delta \left[\sum_j \left(P_j^v \ln P_j^v - P_j^v \ln P_j^\circ + \alpha P_j^v + \beta P_j^v E_j^v \right) \right] \\ &= \sum_j \delta P_j^v \left(1 + \ln \frac{P_j^v}{P_j^\circ} + \alpha + \beta E_j^v \right). \end{aligned} \tag{2.66}$$

Therefore,

$$- \ln \left(\frac{P_j^v}{P_j^\circ} \right) = I(j) = (1 - \alpha) + \beta E_j^v. \tag{2.67}$$

Indeed this means a 1st-order (linear) relationship for surprisal. In cases where L includes the 2nd momentum term, a surprisal would become 2nd order.

2.7 Historical Background

The TPEPICO studies on fundamentals of mass spectrometry were conducted under Drs. Gerry G. Meisels (past President, the American Society for Mass Spectrometry, ASMS), Michael L. Gross (Professor, Washington University), and active and stimulating discussions with the late Chava Lifshitz (Professor of Emeritus, Hebrew University) (she made great contributions in mass spectrometry; regretfully, she lost her decades-long struggle with cancer on March 1, 2005) and Tomas Baer (Professor, University of North Carolina) and collaborators in ASMS during the 1980s. Regarding theoretical and experimental challenges in Japan, TN had been guided under Drs. Kozo Hirota (Professor of Emeritus, Osaka University), the late Toshikazu Tsuchiya and Yoshio Niwa (AIST, Japan), and Hiroshi Matsumoto (past President, Thermo Fisher Scientific, Japan) in photoelectron spectroscopy and mass spectrometry from the early 1970s to 1990s. TN especially thanks Dr. Andrew J. Alpert (President, PolyLC Inc., USA) for his valuable suggestions in this manuscript.

References

1. Rice OK, Ramsperger HC (1928) J Am Chem Soc 50:617–620
2. Kassel LS (1928) J Phys Chem 32:1065–1079
3. Marcus RA (1951) J Phys Colloid Chem 55:894–908
4. Forst W (1973) Theory of unimolecular reaction. Academic, New York
5. Robinson PJ, Holbrook KA (1972) Unimolecular reaction. Wiley, New York
6. Hase WL (1976) Unimolecular reactions. In: Miller WH (ed) Dynamics of molecular collisions part B. Plenum Press, New York
7. Bunker DL (1966) Theory of elementary gas reaction rates. Pergamon Press, New York
8. Rosenstock HM, Wallenstain HB, Warlhaftig AL, Eyring H (1952) Proc Natl Acad Sci U S A 38:667–678
9. Haney MA, Franklin JL (1968) J Chem Phys 48:4093–4097
10. Sztaray B, Bodi A, Baer T (2010) J Mass Spectrom 45:1233–1245
11. Brehm B, von Puttkamer E (1967) Z Naturforsch A22:8
12. Eland JHD (1972) Int J Mass Spectrom Ion Process 8:143–151
13. Niwa Y, Nishimura T, Nozoye H, Tsuchiya T (1979) Int J Mass Spectrom Ion Phys 30:63–73
14. Stockbauer R (1973) J Chem Phys 58:3800–3815
15. Werner AS, Baer T (1975) J Chem Phys 62:2900–2910

16. Batten CF, Taylor JA, Tsai BP, Meisels GG (1978) J Chem Phys 69:2547–2552
17. Révész A, Szepes L, Baer T, Sztáray B (2010) J Am Chem Soc 132:17795–17803
18. Shuman NS, Johnson M, Stevens WR, Harding ME, Stanton JF, Baer T (2010) J Phys Chem A 114:10016–10023
19. Cooks RG, Beynon JH, Caprioli RM, Lester GR (1973) Metastable ion. Elservier, Amsterdam
20. Klots C (1971) J Chem Phys 75:1526–1532
21. Chesnavitch WJ, Bowers MT (1977) J Chem Phys 66:2306–2315
22. Beynon JH, Gilbert JR (1984) Application of transition state theory to unimolecular reactions. Wiley, Chichester
23. Levine RD, Bernstein RB (1987) Molecular reaction dynamics and chemical reactivity. Oxford University Press, New York
24. Smith IWM (1976) Kinetics and dynamics of elementary gas reactions. Butterworths, London, p 129
25. Langevin P (1905) Ann Chim Phys Ser 8(5):245–288
26. Nishimura T, Das PR, Meisels GG (1986) J Chem Phys 84:6190–6199
27. Miller WH (1976) J Chem Phys 65:2216–2223
28. Das PR, Nishimura T, Meisels GG (1985) J Phys Chem 89:2808–2812
29. Nishimura T, Arakawa R (1999) J Mass Spectrom 34:175–183
30. Zha Q, Hayes RN, Nishimura T, Meisels GG, Gross ML (1990) J Phys Chem 94:1286–1290
31. Nishimura T, Meisels GG, Niwa Y (1989) J Chem Phys 91:4009–4018
32. Widoim B (1965) J Chem Phys 43:3892–3897
33. Domb C, Hunter DL (1965) Proc Phys Soc 86:1147–1151
34. Miller BE, Baer T (1984) Chem Phys 85:39–45
35. Jaynes ET (1963) Statistical physics, Brandeis Lectures, vol 3. Benjamin, New York, p 81
36. Bernstein RB (1982) Chemical dynamics via molecular beam and laser techniques. Oxford University Press, New York, Chapter 9
37. Shannon CE, Weaver W (1949) Mathematical theory of communication. University of Illinois Press, Urbana
38. Nishimura T, Meisels GG, Niwa Y (1991) Bull Chem Soc Jpn 64:2894–2900

http://www.springer.com/978-1-4614-7232-2

Fundamentals of Mass Spectrometry
Hiraoka, K. (Ed.)
2013, VII, 239 p. 138 illus., 57 illus. in color., Hardcover
ISBN: 978-1-4614-7232-2